Dynamical Link between the Barents–Kara Sea Ice and the Arctic Oscillation

XIAO-YI YANG

State Key Laboratory of Marine Environmental Science, and College of Ocean and Earth Sciences, Xiamen University, Xiamen, China

XIAOJUN YUAN AND MINGFANG TING

Lamont-Doherty Earth Observatory, Columbia University, Palisades, New York

(Manuscript received 22 September 2015, in final form 8 March 2016)

ABSTRACT

The recent accelerated Arctic sea ice decline has been proposed as a possible forcing factor for midlatitude circulation changes, which can be projected onto the Arctic Oscillation (AO) and/or North Atlantic Oscillation (NAO) mode. However, the timing and physical mechanisms linking AO responses to the Arctic sea ice forcing are not entirely understood. In this study, the authors suggest a connection between November sea ice extent in the Barents and Kara Seas and the following winter's atmospheric circulation in terms of the fast sea ice retreat and the subsequent modification of local air–sea heat fluxes. In particular, the dynamical processes that link November sea ice in the Barents and Kara Seas with the development of AO anomalies in February is explored. In response to the lower-tropospheric warming associated with the initial thermal effect of the sea ice loss, the large-scale atmospheric circulation goes through a series of dynamical adjustment processes: The decelerated zonal-mean zonal wind anomalies propagate gradually from the subarctic to midlatitudes in about one month. The equivalent barotropic AO dipole pattern develops in January because of wave–mean flow interaction and firmly establishes itself in February following the weakening and warming of the stratospheric polar vortex. This connection between sea ice loss and the AO mode is robust on time scales ranging from interannual to decadal. Therefore, the recent winter AO weakening and the corresponding midlatitude climate change may be partly associated with the early winter sea ice loss in the Barents and Kara Seas.

1. Introduction

Arctic sea ice cover has been declining throughout the calendar year at an unprecedented pace since the 1990s (Comiso et al. 2008), in sharp contrast to the all-season increase of Antarctic sea ice (Simmonds 2015). A series of positive feedback processes has been proposed to interpret the accelerated decline of Arctic sea ice under the global warming background, indicating a close coupling of the local ice–atmosphere–ocean system (Screen and Simmonds 2010; Stroeve et al. 2012). Even though the observed sea ice retreat has been underestimated in the coupled global climate models, the central Arctic Ocean is predicted to be ice free in summer as early as the middle of this century (Stroeve et al. 2012; Massonnet et al. 2012). Such a fast ice retreat has drawn increasingly more attention from the scientific community to evaluate the possible climate impact resulting from the Arctic sea ice loss.

As an integral part of Earth's climate system, the Arctic sea ice cover plays an important role in the Northern Hemispheric high-latitude surface energy budget through modulating surface albedo as well as the turbulent heat and momentum fluxes at the ocean–atmosphere interface (Serreze et al. 2007). The direct atmospheric responses to the Arctic sea ice loss include increased lower-tropospheric heating and moisture content, reduced vertical static stability, and the stretching of Arctic air columns that results in the slackening of the poleward thickness gradient (Francis et al. 2009; Overland and Wang 2010). Aside from the local thermodynamic effects, the Arctic sea ice variations have the potential to influence the midlatitude

Corresponding author address: Xiao-Yi Yang, C3-418, Xiping building, Xiang An Campus, Xiamen University, Xiang An Nan Road, Xiamen, Fujian 361102, China.
E-mail: xyyang@xmu.edu.cn

DOI: 10.1175/JCLI-D-15-0669.1

climate and weather (see review papers by Serreze et al. 2007; Budikova 2009; Bader et al. 2011; Vihma 2014). The possible influences of the Arctic sea ice can be summarized as follows: 1) creating a warm Arctic–cold continents (Eurasia and part of North America) pattern (Honda et al. 2009; Petoukhov and Semenov 2010; Overland et al. 2011; Inoue et al. 2012; Mori et al. 2014); 2) changing the location and intensity of storm tracks and storminess (Murray and Simmonds 1995; Seierstad and Bader 2009; Simmonds and Keay 2009); 3) causing more frequent and long-lasting midlatitude extreme weather conditions (Francis and Vavrus 2012; Cohen et al. 2014a) in spite of the controversy regarding the artifact and randomness of the analysis method (e.g., Barnes 2013); and 4) weakening and warming of the stratospheric polar vortex (Kim et al. 2014). The atmospheric responses in all of the above studies tend to be related to the changes in the Arctic Oscillation (AO), or its regional manifestation, the North Atlantic Oscillation (NAO) mode. Nevertheless, the relatively short observational record and the low signal-to-noise ratio in the midlatitude make it difficult to interpret the physical linkage between Arctic sea ice and AO/NAO modes (Screen et al. 2013, 2014). Because of the complexity of sea ice–atmosphere coupling, the large-scale atmospheric circulation response to the underlying sea ice change is often investigated using model sensitivity experiments. By prescribing the Atlantic sea ice anomalies in an atmospheric general circulation model (AGCM), Deser et al. (2004) reported that the atmospheric circulation response to sea ice change resembles the AO/NAO modes. The sea ice loss to the east of Greenland corresponds to a weaker and southward-shifted storm track over the North Atlantic, which is consistent with the negative AO/NAO response (Magnusdottir et al. 2004; Alexander et al. 2004; Liptak and Strong 2014). Moreover, the negative AO/NAO response to the reduced sea ice condition has been reported in observational studies (Honda et al. 2009; Wu and Zhang 2010). Strong et al. (2009) and Strong and Magnusdottir (2011) further suggested that a negative sea ice–atmosphere feedback over the Atlantic sector can be detected in both observational data and global climate models: a positive phase of AO/NAO favors increased (reduced) sea ice to the west (east) of Greenland through horizontal sea ice and temperature advection (Rigor et al. 2002; Zhang et al. 2003; Yang and Yuan 2014), and the sea ice anomalies in turn force a negative AO/NAO response.

The fundamental effect of sea ice on the winter atmospheric circulation lies in its capacity to mediate surface turbulent heat fluxes. With large air–sea temperature difference during the winter, the turbulent heat flux from an open ocean may reach 300–500 $\mathrm{W\,m^{-2}}$, which is almost two orders of magnitude larger than that through the ice (Andreas 1980; Simonsen and Haugan 1996). One of the key regions of Arctic sea ice variability is the Barents–Kara (BK) Seas. The BK Seas are at the main pathway through which the warm Atlantic waters flow into the Arctic Ocean (Schauer et al. 2002). A recent study by Sato et al. (2014) indicated that the ice decline in the BK sector is likely associated with the poleward shift of the Gulf Stream front and increased ocean heat transport into the Barents Sea (Årthun et al. 2012). Even the hemispheric-mean decline in winter sea ice extent is due in large part to the increasing SST in the Barents Sea and adjacent waters (Francis and Hunter 2007). The drastic BK sea ice loss, along with the recent warming of the Atlantic inflow (Polyakov et al. 2004; Spielhagen et al. 2011), could induce an increase of turbulent heat flux from the ocean to the atmosphere, as shown in Årthun et al. (2011) and Koenigk and Brodeau (2014). A number of studies have highlighted the BK sea ice as a crucial factor in influencing the recent Arctic climate change (Petoukhov and Semenov 2010; Smedsrud et al. 2013; Yang and Yuan 2014). In particular, the BK sea ice variation is capable of impacting the air pressure over Scandinavia (Koenigk et al. 2009), the winter cyclone track (Inoue et al. 2012), the stratospheric polar vortex intensity (Kim et al. 2014), and AO/NAO modes (Liptak and Strong 2014).

In spite of numerous efforts to explore the sea ice–AO relation, there is still a lack of consensus on the polarity of the response to sea ice reduction in the modeling studies, from positive phase (Strey et al. 2010; Orsolini et al. 2012), to no significant change (Screen et al. 2014), and to negative phase of AO/NAO (e.g., Peings and Magnusdottir 2014). The timing of the AO/NAO pattern's establishment also differs greatly from early winter (November and December) (Screen et al. 2013), to midwinter (January and February) (Deser et al. 2010; Peings and Magnusdottir 2014), and then to late winter (March) (Seierstad and Bader 2009), possibly as a result of the varying model forcing and experimental designs. In the observational studies, the large spatial extent and the temporally continuous sea ice loss make it difficult to ascertain the key geographical region and timing of the sea ice forcing to the atmosphere. Furthermore, the dominant physical pathways through which sea ice may influence the midlatitude atmospheric circulation are not completely understood despite some suggested processes (Mori et al. 2014; Kim et al. 2014). Cohen et al. (2014a) summarized the current understanding of the three pathways linking the Arctic to the midlatitude: storm tracks, the jet stream, and the planetary waves. They further stressed that large uncertainties and

debates still exist "because of incomplete knowledge of how high-latitude climate change influences these phenomena" (Cohen et al. 2014a, p. 627). In this study, we identify the November BK sea ice as a possible candidate that, through local thermal effect and remote wave–mean flow interaction, can influence the midwinter AO. Through a sequence of processes involving baroclinic response, barotropic adjustment, and the stratosphere–troposphere coupling, the atmospheric responses to sea ice loss are relayed from the Arctic to midlatitudes and from the lower troposphere up to the stratosphere with the time progression from November to February. Our results indicate that the weakening of AO in the recent two decades could be at least partially attributed to the accelerated BK sea ice retreat in November. Thus, BK sea ice can be a potential predictor for winter AO and the related surface climate, as well as for future Northern Hemisphere (NH) climate change.

Our study is unique in exploring the sequence of physical processes to reveal the possible dynamic adjustment of the atmospheric circulation to the underlying sea ice forcing through observational analysis. The outline of the work is as follows: The data and methods used in the study are discussed in section 2. In section 3, the November sea ice index for the Barents and Kara Seas is defined, and the effect of BK sea ice decline on the Arctic warming is established. Next the winter extratropical atmospheric circulation variability associated with the sea ice anomalies is described in section 4, followed in section 5 by the wave–mean flow interaction mechanism, which is used to interpret the internal atmospheric dynamical adjustment processes. Finally, section 6 presents a synthesis of all involved dynamic processes and discussions.

2. Data and methods

The sea ice concentration (SIC) dataset was developed by the National Aeronautics and Space Administration team using the *Nimbus-7* SMMR (1978–87), DMSP SSM/I (1987–2009), and DMSP SSMIS (2008–present) satellite passive microwave radiances on a 25 km × 25 km polar stereographic grid (Cavalieri et al. 2013). The monthly mean data of SIC for 35 years from January 1979 to December 2013 are used in this study.

The monthly AO and NAO indices are downloaded from the NOAA/Climate Prediction Center file server (ftp://ftp.cpc.ncep.noaa.gov). The monthly and daily meteorological fields including air temperature, geopotential height, horizontal and vertical velocities, and surface latent and sensible heat fluxes are obtained from the ERA-Interim dataset (Dee et al. 2011), with a horizontal resolution of 1.5° × 1.5° and 37 pressure levels from 1000 to 1 hPa.

The Eliassen–Palm (EP) flux on a latitude–pressure section is computed from the following formula:

$$(F_\varphi, F_p) = p\cos\varphi \times \left(-\overline{[u'v']}, \frac{2\Omega\sin\varphi}{S}\overline{[v'T']}\right).$$

Here u, v, T, φ, p, and Ω are the zonal and meridional winds, air temperature, latitude, pressure, and Earth's rotation angular velocity, respectively. The static stability parameter S is defined as $S = (\partial\hat{T}/\partial z) + (\kappa\hat{T}/H)$, where $H = -(\hat{z}/\ln p)$ is the scale height, $\kappa \approx 0.286$ is a constant, and the hat represents the area average in the extratropical Northern Hemisphere (poleward of 20°N). The square bracket stands for zonal mean, and the overbar stands for time mean. Prime denotes the deviation from zonal mean for the stationary wave EP fluxes or the deviation from monthly mean for the transient eddy EP fluxes. The meridional and vertical components of EP flux represent the wave momentum and heat fluxes as well as the wave energy propagation in the meridional and vertical directions. The EP flux divergence $\nabla\cdot\mathbf{F} = \partial F_\varphi/\partial y + \partial F_p/\partial z$ is equal to the poleward flux of quasigeostrophic potential vorticity $\overline{v'q'}$. According to the nonfrictional quasigeostrophic transformed Eulerian mean (TEM) equations, $\partial\overline{u}/\partial t = f_0\overline{v}^* + \overline{v'q'}$, the meridional potential vorticity flux could be an important forcing factor for the acceleration and deceleration of the zonal-mean zonal flow [for details, refer to Vallis (2006, chapter 7)]. Therefore, the EP flux divergence is an excellent diagnostic tool for wave–mean flow interaction, with EP flux divergence (convergence) tending to accelerate (decelerate) the zonal-mean zonal flow.

One of the relevant sea ice indices used in the study, the November BK sea ice index (NovBASI) is obtained by first summing up the areas of all grid boxes covered with at least 15% sea ice concentration in the Barents and Kara Seas (70°–82°N, 15°–103°E) in November and then normalizing the time series with its standard deviation. Because of the large trend in this index, we further constructed the detrended NovBASI by removing the 1979–2013 linear trend from the NovBASI. The regression coefficients of the zonal-mean atmospheric fields (e.g., geopotential height H, air temperature T, and zonal wind U) onto the sea ice index are estimated using the least-squares fit after removing all linear trends, as $R(\varphi, p) = \overline{\mathrm{SI}'(t)A'(\varphi, p, t)}/\overline{\mathrm{SI}'(t)^2}$, where $\mathrm{SI}(t)$ is the sea ice index at time t and $A(\varphi, p, t)$ is the zonal-mean atmospheric variable on a meridional plane. The overbar (prime) denotes the time mean (the deviation from the time mean). The statistical significance of the regression coefficients is assessed using a Student's t test following Bretherton et al. (1999). To explore the time evolution of atmospheric circulation in response to the initial sea ice forcing, composite analyses

are applied to the daily data as well as the monthly data-based on the high and low sea ice index years. Here, all daily data are preprocessed by a 15-day running mean in order to filter out the higher-frequency fluctuations.

We follow Santer et al. (2000) to estimate the linear trend and its significance level by taking account of the lag-1 autocorrelation of the time series. The trend that is congruent to the sea ice decline is computed as $\alpha R(\varphi, p)$, where α is the sea ice trend and $R(\varphi, p)$ is the regression coefficients between the detrended atmospheric variables and the sea ice index. Our method differs slightly from the method used by previous studies, such as Thompson et al. (2000) and Zhou and Li (2008). In contrast to these previous studies, we used detrended data for calculating the regression coefficients. This process can effectively rule out the inflation of the regression coefficient by coincident trends that may lack physical connection but not change the pattern qualitatively. The atmospheric circulation trends could be significantly attributed to the sea ice change when the regression coefficients between them are significant at the 95% confidence level based on the Student's t test. Note the trend congruence method, though statistically reasonable, is based on an implicit assumption that the covariation associated with the high- and low-frequency fluctuations applies physically and translates meaningfully to the context of trends. Therefore, care must be taken in using this method to interpret long-term climate change.

3. The key region and critical timing of sea ice forcing

a. *Sea ice trends and interannual variability*

The spatial pattern of the annual-mean sea ice concentration trends during the period of 1979–2013 is exhibited in Fig. 1a. For the last three decades, the negative sea ice trends dominate the entire Arctic region, except for the Bering Sea and the northern Greenland Sea. The most dramatic ice loss occurs in the BK Seas, with a decline of over 12% decade^{-1}. The longitude–month distribution of sea ice trends averaged for 70°–85°N reveals that the sea ice decline trends in the BK sector persist throughout the year, in contrast to the strong seasonality of sea ice trends in the Chukchi, East Siberian, and Laptev Seas (Fig. 1b). In addition to the long-term trend, the interannual variability of Arctic sea ice in wintertime is also dominated by the BK sea ice anomalies, as represented by the maximum SIC standard deviations in BK sectors from November to May (Fig. 1b, black thin contours). The BK area-mean surface net heat flux trends and standard deviations for each calendar month during the period of 1979–2013 are displayed in Fig. 1c. In the wintertime from October to May, the BK surface heat fluxes from the ocean to atmosphere exhibit increased trends and large interannual variations, both of which peak in the month of November. The greatest increase of BK surface heat flux in November may result from the combination of the open water area expansion associated with the local sea ice retreat and the seasonally dependent air–sea temperature differences. Although Koenigk et al. (2015) suggested that November sea ice in BK Seas has the largest impact on NAO, the trends and variability of surface fluxes presented in Fig. 1b provide evidence why November is the critical month. In the annual cycle, BK mean surface heat flux is upward throughout the year (except for July) (figure not shown), the negative heat flux trends in summer months are likely due to the northward shift of the ice edge and the drawdown of ocean heat by the excessive ice melting.

b. *Construction of November Barents and Kara sea ice index*

Model sensitivity experiments by Deser et al. (2010) found that the seasonal cycle of the climate response to sea ice anomalies followed that of the net surface heat flux rather than that of the sea ice itself. The peaks of BK surface heat flux standard deviation and trend in November (Fig. 1c) correspond to the westward shift of maximum SIC anomalies from the Chukchi and East Siberian Seas in summertime to the BK sector in wintertime (Fig. 1b), designating November as the critical time of sea ice forcing to the winter atmospheric circulation. Therefore, we establish a November BK sea ice index to investigate the impact of sea ice on the overlying atmospheric circulation. Figure 2a illustrates the normalized NovBASI, as discussed in section 2. In recent decades, the November BK sea ice extent retreats at an accelerated rate, with the trend slopes ranging from -0.482 decade^{-1} during 1979–2013, to -1.179 decade^{-1} during 1988–2013, and further to -1.952 decade^{-1} during 1998–2013 (Fig. 2a). After the linear trend for the entire period is removed from the NovBASI, the detrended index exhibits a strong variation on the decadal time scale, with positive anomalies in the 1990s and negative anomalies in the 1980s and the recent decade (Fig. 2b). The power spectrum analysis of the NovBASI yields significant peaks at the interannual time scale (3–4 yr) and decadal periods at the 95% confidence level against the red-noise spectrum (figure not shown). Accordingly, a harmonic analysis of Fourier transforms is applied to derive the decadal (longer than 10-yr period) and interannual (2–10-yr period) parts of NovBASI (Figs. 2b,c). This way, we linearly separate the NovBASI into three components: a long-term trend, a decadal oscillation

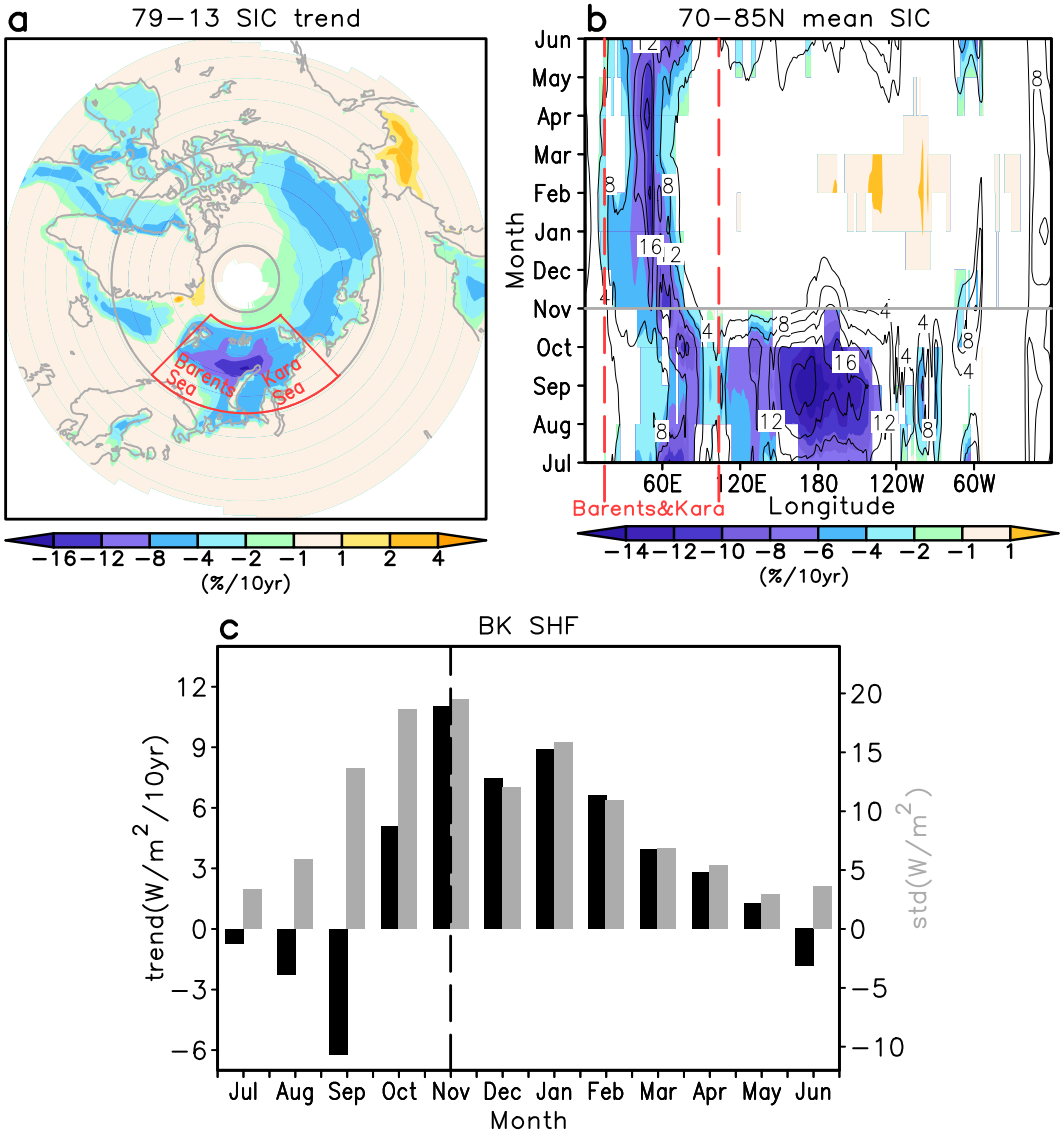

FIG. 1. (a) Linear trends of annual-mean sea ice concentration during the period of 1979–2013. The red solid lines mark the Barents and Kara Seas. (b) Linear trends (color shading) and standard deviation (black contours) of 70°–85°N [the gray ring in (a)] mean sea ice concentration for each month. Only the positive (negative) trends that exceed the 95% confidence level are shown. Thick red dashed lines define the longitudinal extension of the Barents and Kara Seas. (c) Linear trends (black bars) and standard deviation (gray bars) of BK mean net surface turbulent heat flux for each calendar month. The dashed line marks the month of November.

(low-NovBASI), and the interannual variability (hi-NovBASI). Because of the nonlinearity of the sea ice trend over the satellite era, linear detrending of the NovBASI time series with a slower decline in the first half (pre-1998) and faster decline in the second half (post-1998) will automatically lead to a detrended time series with some decadal-scale fluctuations. Thus the low-NovBASI on decadal and longer time scales may contain the factitious low-frequency oscillation as a result of the linear detrending process. In addition, the decadal variability observed in this study may be partially due to anthropogenic forcing as well as natural decadal variations in sea ice extent. In this study, the dynamic link between the winter atmospheric circulation and the Arctic sea ice anomalies is investigated through either linear regression or composite methods mostly based on the hi-NovBASI (Fig. 2c), unless otherwise stated. A total of 17 out of the 35 years is selected on the threshold of plus or minus one standard deviation of hi-NovBASI. The compositing analysis is not sensitive to the sample size, as the results are qualitatively unchanged by varying the

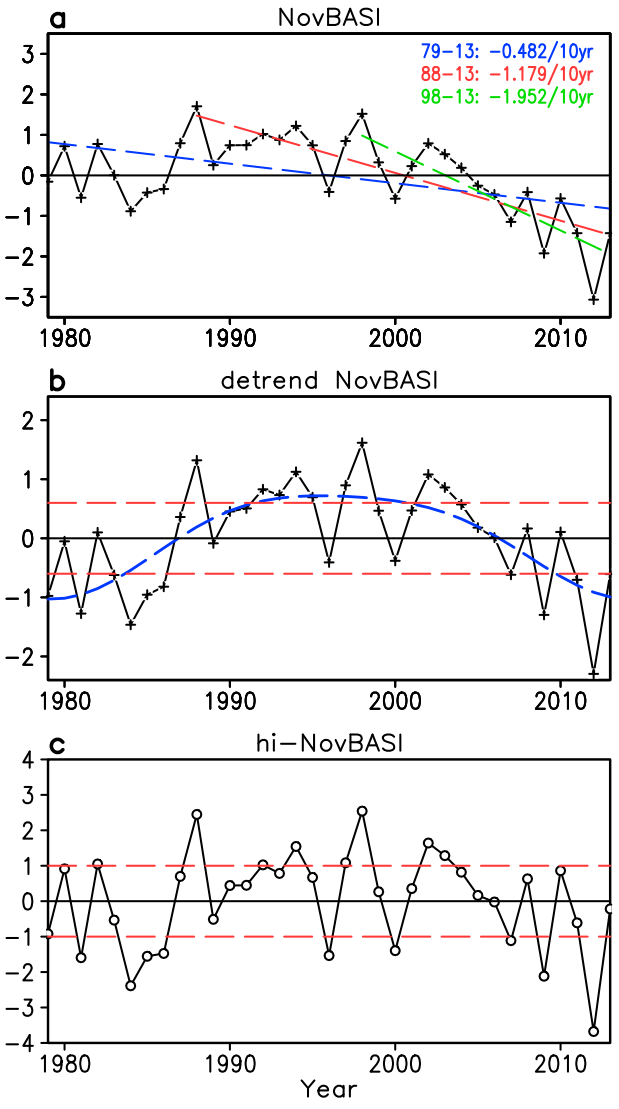

FIG. 2. (a) Normalized NovBASI, with the dashed lines denoting the downward trend for the periods of 1979–2013 (blue), 1988–2013 (red), and 1998–2013 (green); (b) the detrended NovBASI with the 1979–2013 linear trend subtracted. The dashed blue line is the multidecadal component (10–35 yr) of NovBASI (low-NovBASI) derived by the harmonic analysis of Fourier transforms. The dashed red lines denote ±0.6 std dev of the low-NovBASI. (c) The interannual component (2–10 yr) of NovBASI (hi-NovBASI) derived by the harmonic analysis of Fourier transforms. The dashed red lines denote ±1.0 std dev of the hi-NovBASI.

threshold to ±1.25 or ±0.75 standard deviation (figures not shown). Also, the low-NovBASI is applied to validate the robustness of the NovBASI–AO connection on decadal time scales.

c. Direct thermal effect of Barents and Kara sea ice

The November BK sea ice anomalies may act as a diabatic heating source to the overlying atmosphere through creating more open water area and increasing the local heat flux from the ocean to the atmosphere. The direct thermal forcing of November BK sea ice loss and the role of such loss on the recent Arctic amplification of global warming are illustrated in Fig. 3, which shows the zonal-mean 2-m air temperature trends for the period 1979–2013 (Fig. 3a) and the trends congruent to the NovBASI (Fig. 3b). From late fall through winter, the warming trends amplified poleward, but their domain shrank with the season. Almost no warming tendency appeared in midwinter (December–January) south of 60°N (Fig. 3a). To estimate how much of this Arctic warming is associated with the November BK sea ice loss, we then regressed the detrended zonal-mean temperature anomalies onto the detrended NovBASI and multiplied the regression coefficients with the actual linear trend value of NovBASI to obtain the congruent Arctic warming trend to the sea ice trend. The temperature trends congruent to the NovBASI (Fig. 3b) bear some resemblance to the observed trends, but the warming is confined to north of 70°N, and there are significant cooling trends south of 70°N from December to March. We also examined the surface air temperature trends in each grid box for the winter months. The result exhibits a westward shift of the maximum Arctic warming with season, from the Chukchi–East Siberian Seas (October–November) to the BK Seas (December–February) (figures not shown). This matches the westward shift of Arctic sea ice variability from summer to winter (Fig. 1b), suggesting a possible positive feedback in the high latitudes: Arctic warming in the late summer–early winter, November BK sea ice loss, enhanced heat flux from the ocean to the atmosphere, and further Arctic warming in the midwinter. This local atmosphere–ice feedback can be verified in the lead–lag correlation between the NovBASI and surface air temperature as well as the net surface heat flux anomalies: The atmospheric warming over the BK Seas and the subsequent reduced ocean heat loss in October are followed by the November BK sea ice decline (Fig. 3c), which, in turn, favors the increased ocean heat loss to atmosphere and the Arctic warming in December (Fig. 3d). However, the significant midlatitude cooling trends in midwinter cannot be directly attributed to the sea ice thermal forcing but are involved in the atmospheric dynamic adjustment processes.

4. Large-scale atmospheric circulation response

To explore the impact of November BK sea ice loss to the large-scale atmospheric circulation on the interannual time scale, we regressed December–February zonal-mean geopotential height and air temperature anomalies onto the hi-NovBASI (Fig. 4). All the regression coefficients are multiplied by −1 so that the

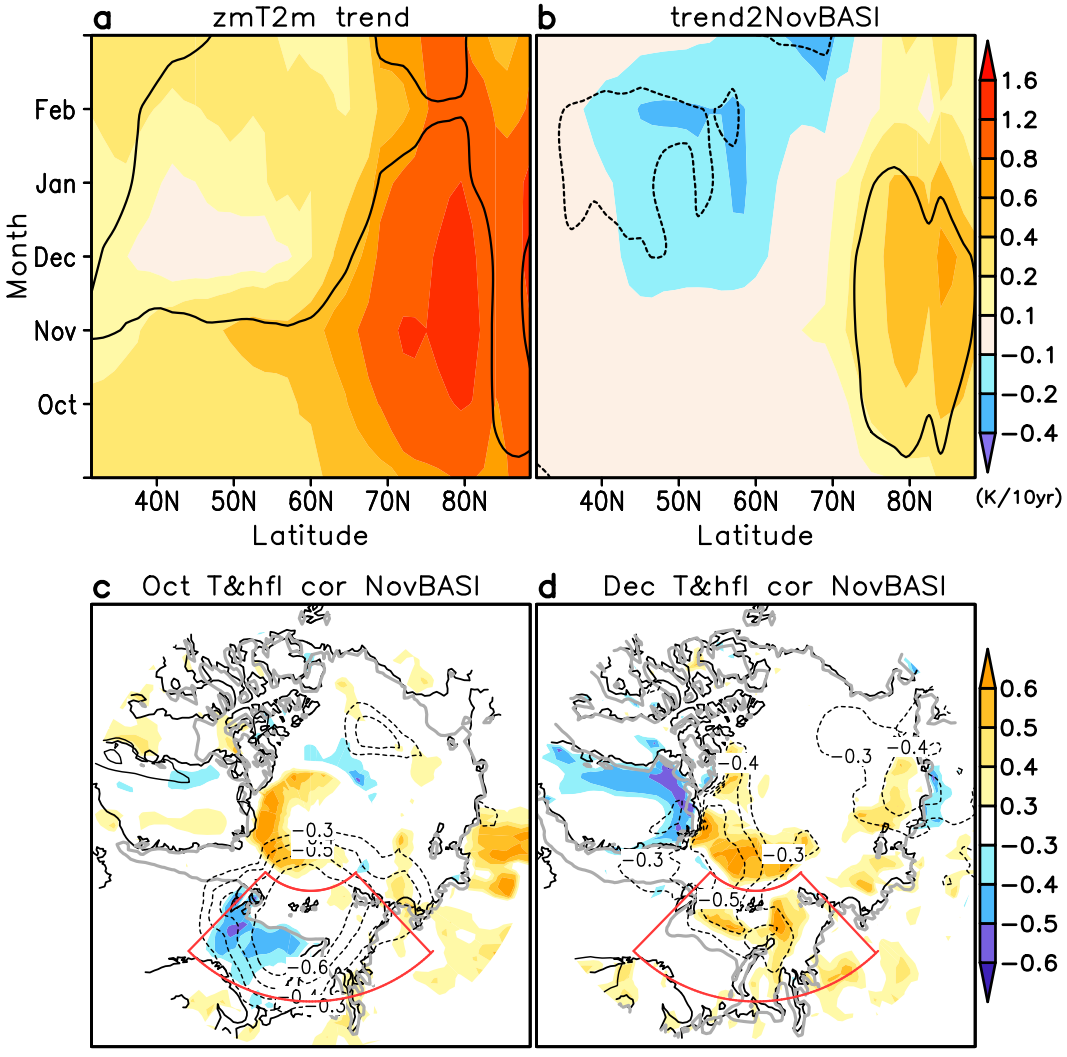

FIG. 3. (a) The 1979–2013 zonal-mean 2-m air temperature trends for each calendar month from September to March. (b) Monthly trends of zonal-mean 2-m air temperature that is congruent with the NovBASI. Solid (dashed) lines encircle the positive (negative) trends that exceed the 95% confidence level. Here, the trends congruent to NovBASI are estimated by multiplying the actual linear trend value of NovBASI with the regression coefficients of detrended zonal-mean 2-m air temperature anomalies onto the detrended NovBASI. (c) Lag correlation between the NovBASI and the October surface air temperature (black contours) and the October net surface heat flux (color shading). The contour intervals are −0.6, −0.5, −0.4, −0.3, 0.3, 0.4, 0.5, and 0.6. The thick gray lines mark the October climatological sea ice edges (SIC ≥ 15%). The Barents and Kara Seas are enclosed by red thick lines. (d) As in (c), but for the correlation between the NovBASI and the December surface air temperature and the December net surface heat flux. Note that the positive anomalies of surface heat flux represent the decreased ocean heat loss to the overlying atmosphere, and vice versa.

anomalies correspond to the minus one standard deviation of hi-NovBASI. The November sea ice loss tends to be associated with anomalous high pressure north of 60°N and anomalous low pressure south of 60°N in December (Fig. 4a). The significant positive anomalies of zonal-mean geopotential height extend upward from the lower troposphere, which is consistent with a significant polar warming associated with November sea ice loss (Fig. 4d). The near-surface Arctic warming subsides in January (Fig. 4e). Correspondingly, the tropospheric positive geopotential height anomalies north of 60°N decrease in magnitude but are still statistically significant, while the negative anomalies in the midlatitude at tropospheric levels become statistically significant (Fig. 4b). This dipole geopotential height pattern indicates the meridional seesaw relation between the Arctic and subarctic air mass, denoting the negative phase of the AO mode. In February, the dipole

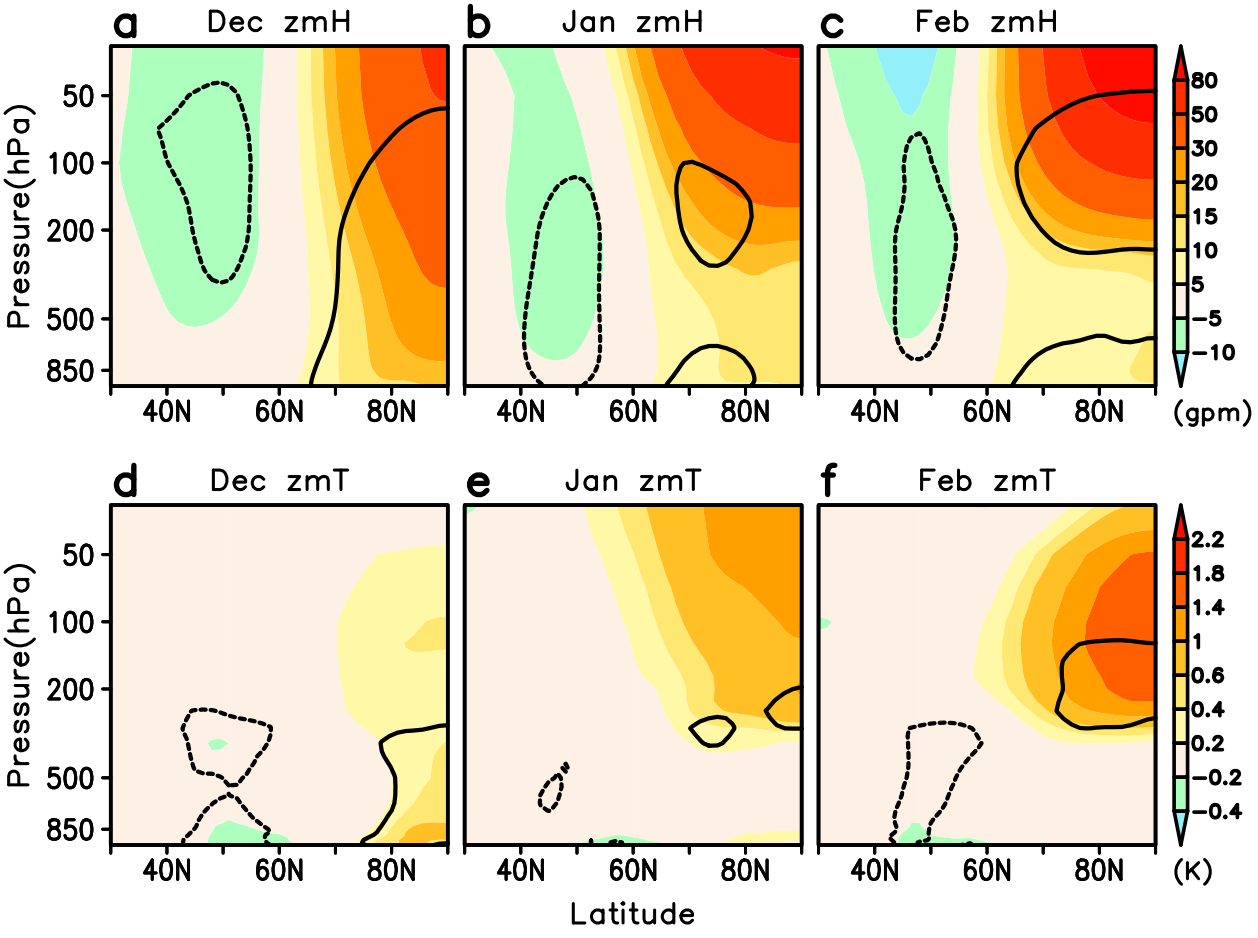

FIG. 4. Lag-regression coefficients of zonal-mean geopotential height anomalies in (a) December, (b) January, and (c) February on the hi-NovBASI. The regression coefficients are multiplied by −1 so that the anomalies correspond to −1 std dev of hi-NovBASI. (d)–(f) As in (a)–(c), but for zonal-mean air temperature. Solid (dashed) lines enclose the positive (negative) values that are significant at the 95% confidence level.

pattern of geopotential height anomalies remains stable and extends to the lower stratosphere, along with the warming and weakening of the stratospheric polar vortex (Figs. 4c,f). To further verify the coherence between the NovBASI and the winter polar vortex, we defined a polar vortex index (PVI) by area averaging the geopotential height anomaly over the area north of 70°N. The PVI is normalized by the standard deviation for each pressure level and multiplied by −1 so that the negative (positive) values correspond to the weakening (strengthening) of polar vortex. This PVI definition is similar to that of Kim et al. (2014). Figure 5a shows the regression coefficients of the detrended PVI onto the hi-NovBASI for the wintertime months. The prevailing positive values of regression clearly indicate the weakening (strengthening) of winter polar vortex in accordance with the negative (positive) anomalies of BK sea ice extent. The PVI anomalies mostly locate in the troposphere in December and extend in the lower stratosphere in February, though their magnitudes abate with time (Fig. 5a). On the decadal time scale, however, the polar vortex–NovBASI coherence appears stronger in February than in December, and the only significant regression coefficients emerge in the lower-stratospheric level (Fig. 5b). Hence, the weakening (strengthening) of stratospheric polar vortex in February apparently keeps pace with the negative (positive) anomalies of November BK sea ice both on the interannual time scale and on the decadal time scale.

The zonal-mean zonal wind anomalies associated with the hi-NovBASI (Figs. 6a–c) are highly consistent with the geopotential height and temperature fields (Fig. 4). Arctic warming (Fig. 4d) reduces the meridional thickness gradient, leading to the deceleration of subpolar zonal winds in December (Fig. 6a). The negative zonal wind anomalies shifted southward to about 60°N in January (Fig. 6b). In February, the decelerated polar nighttime jet (Fig. 6c) accompanies the weakening of the stratospheric polar vortex (Fig. 4c). Consequently, the zonal wind dipole pattern with

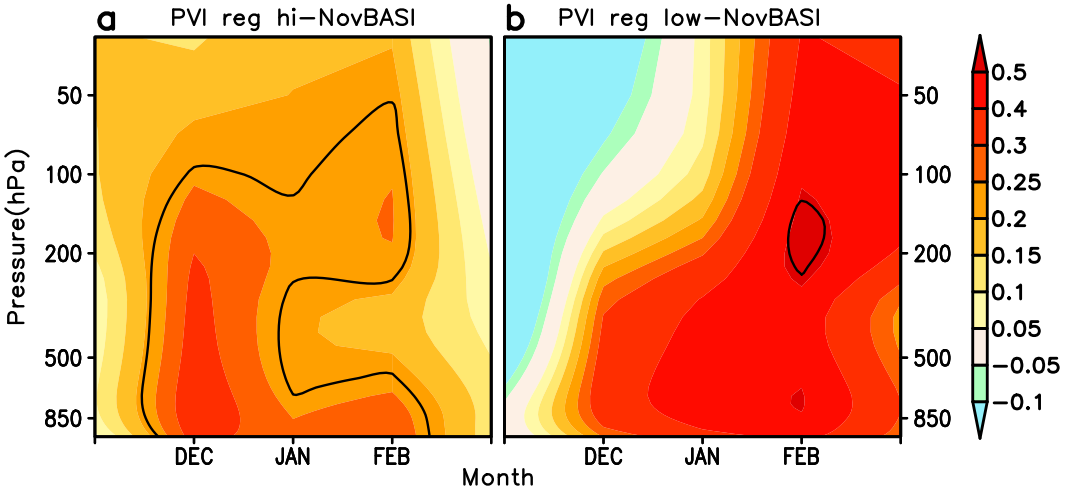

FIG. 5. Regression coefficients of 1979–2013 wintertime monthly detrended PVI (see detailed definition in the text) onto (a) the hi-NovBASI and (b) the low-NovBASI. The black contours indicate the regressions that are significant at the 95% confidence level.

the deceleration at 50°–70°N and the acceleration at 30°–45°N is fully developed from the surface to the stratosphere (Fig. 6c). In contrast, the zonal wind anomalies corresponding to minus one standard deviation of low-NovBASI can be hardly discerned in December and January (Figs. 6d,e). The NovBASI-related zonal wind dipole pattern in the troposphere and the deceleration of stratospheric polar nighttime jet in February, however, are also validated on the decadal time scale (Fig. 6f).

The robustness of delayed atmospheric circulation response to the November BK sea ice on the interannual time scale can be further verified through the composite analysis method. The composite patterns of zonal-mean zonal wind based on hi-NovBASI resemble the regression patterns, but with larger amplitude of anomalies (Figs. 7a–c). The composites of the winter meridional circulation anomalies based on hi-NovBASI are shown in Figs. 7d–f. The meridional polar cell enhances significantly in December, with anomalous ascent in the midlatitude and descent near the North Pole (Fig. 7d). Although the anomalous polar cell seems to break down in midwinter as a result of the weakening of the midlatitude updraft, the northern anomalies at its lower branch sustain in magnitude and position for the whole winter (Figs. 7e,f). These northerly anomalies may incite the further deceleration of lower-tropospheric zonal winds through the Coriolis effect. It is noteworthy that the strengthening of the polar cell is not thermally driven because the anomalous downdraft at the North Pole is not consistent with the general Arctic warming. The possible mechanism of this anomalous meridional cell will be discussed in the next section.

As the primary leading mode of NH extratropical atmospheric circulation, AO reflects the zonally symmetric seesaw pattern of the Arctic and subarctic air mass, the out-of-phase relation between the zonal wind at 35° and 55°N (Ambaum et al. 2001), and the coupling between the troposphere and stratospheric polar vortex (Baldwin and Dunkerton 2001; Cohen et al. 2007). Our analyses indicated that the midwinter geopotential height and zonal-mean zonal wind dipole patterns, as well as the stratosphere–troposphere coupling associated with the NovBASI, are strongly projected onto the AO/NAO mode. This relation is further validated in Fig. 8a by the significant correlation between the detrended NovBASI and the detrended AO/NAO indices in January and February (Fig. 8a). When applying an 11-yr running mean to the NovBASI, AO, and NAO indices, there appears to be a coherence between the NovBASI and February AO/NAO indices at the decadal time scale, with the upward (downward) tendencies prior to (following) the late 1980s (Fig. 8b). Therefore, the AO–NovBASI connection particularly stands out in February, as they covary not only at the interannual time scale but also at the decadal time scale.

According to the numerical experiments by Deser et al. (2007), the atmospheric response to the Arctic sea ice anomalies is initially baroclinic and gradually adjusts to an equivalent barotropic AO/NAO pattern in 2–2.5 months. Our result supports these modeling results. However, the detailed processes and factors linking the November BK sea ice anomalies with the February AO/NAO mode have not been clearly explained so far. Here, we further explore the atmospheric responses to the underlying sea ice anomalies in terms of mechanisms and their temporal evolution from fall to winter. The 15-day low-pass filtered zonal wind anomalies at 500 hPa

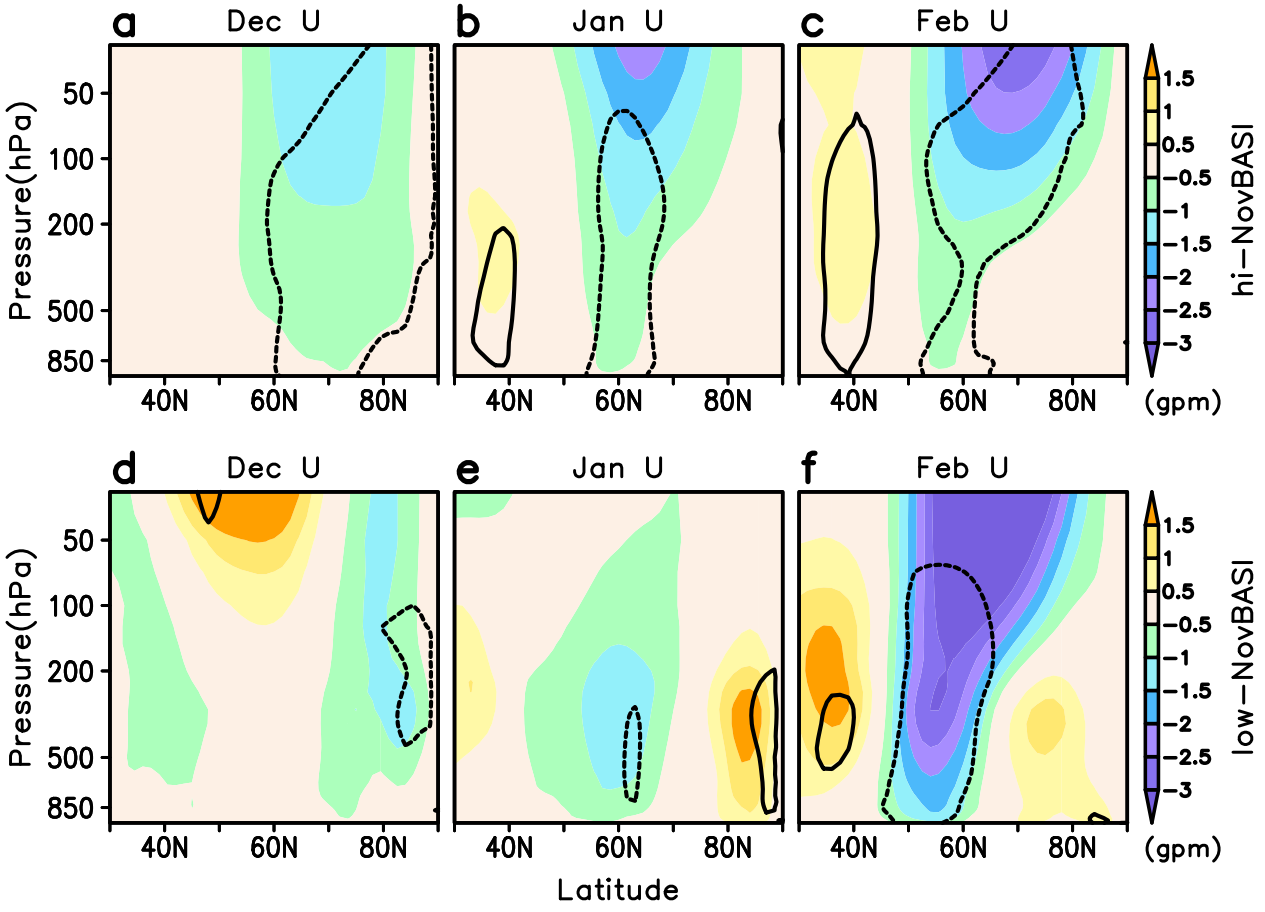

FIG. 6. Lag-regression coefficients of zonal-mean zonal wind anomalies in (a) December, (b) January, and (c) February on the hi-NovBASI. The regression coefficients are multiplied by −1 in order to represent the anomalies corresponding to the −1 std dev of hi-NovBASI. Solid (dashed) lines enclose the positive (negative) values that are significant at the 95% confidence level. (d)–(f) As in (a)–(c), but for lag regressions on the low-NovBASI.

are composited for the low-minus-high hi-NovBASI years (Fig. 9a) to depict the possible atmospheric adjustment process. The November BK sea ice retreat is accompanied by the reversal of the tropospheric zonal wind anomalies at about 80°N, from an anomalous westerly in early November to an anomalous easterly in late November–early December. The early November anomalous westerly corresponds to a cyclonic circulation over the Arctic and the anomalous low pressure over Scandinavia, favoring BK sea ice reduction through enhanced warm temperature advection together with the anomalous high pressure over western Siberia (Fig. 9c). The warming associated with BK ice retreat drives the westerly deceleration by weakening the meridional temperature gradient. Once zonal wind relaxes, the tropospheric circulation becomes less zonal, favoring stronger trough and ridge structure and increased meridional flow (Cohen et al. 2014a). The subsequently enhanced temperature advections facilitate the north–south heat exchange, leading to a weaker meridional temperature gradient and further deceleration of the zonal wind to the south. This positive feedback accounts for the synchronous equatorward shift of negative zonal wind anomalies (Fig. 9a) along with the reduced meridional temperature gradient in December (Fig. 9b). The above inference is well founded in the lead–lag correlations between zonal-mean zonal wind and temperature gradient anomalies (as indicated by the red contours in Figs. 9a,b). The early December temperature gradient at 80°N (the cross marker in Fig. 9b) is positively correlated with the zonal-mean zonal wind anomalies, with the maximum correlation axis tilted southward with time (red contours in Fig. 9a). Similarly, the deceleration of zonal wind at 75°N (the cross marker in Fig. 9a) is associated with the reduced temperature gradient at its equatorward flank (red contours in Fig. 9b). In early January, the positive zonal wind anomalies appear at around 35°N, aligning with the stabilization of negative anomalies at around 55°–60°N (Fig. 9a). This tropospheric zonal wind dipole pattern is

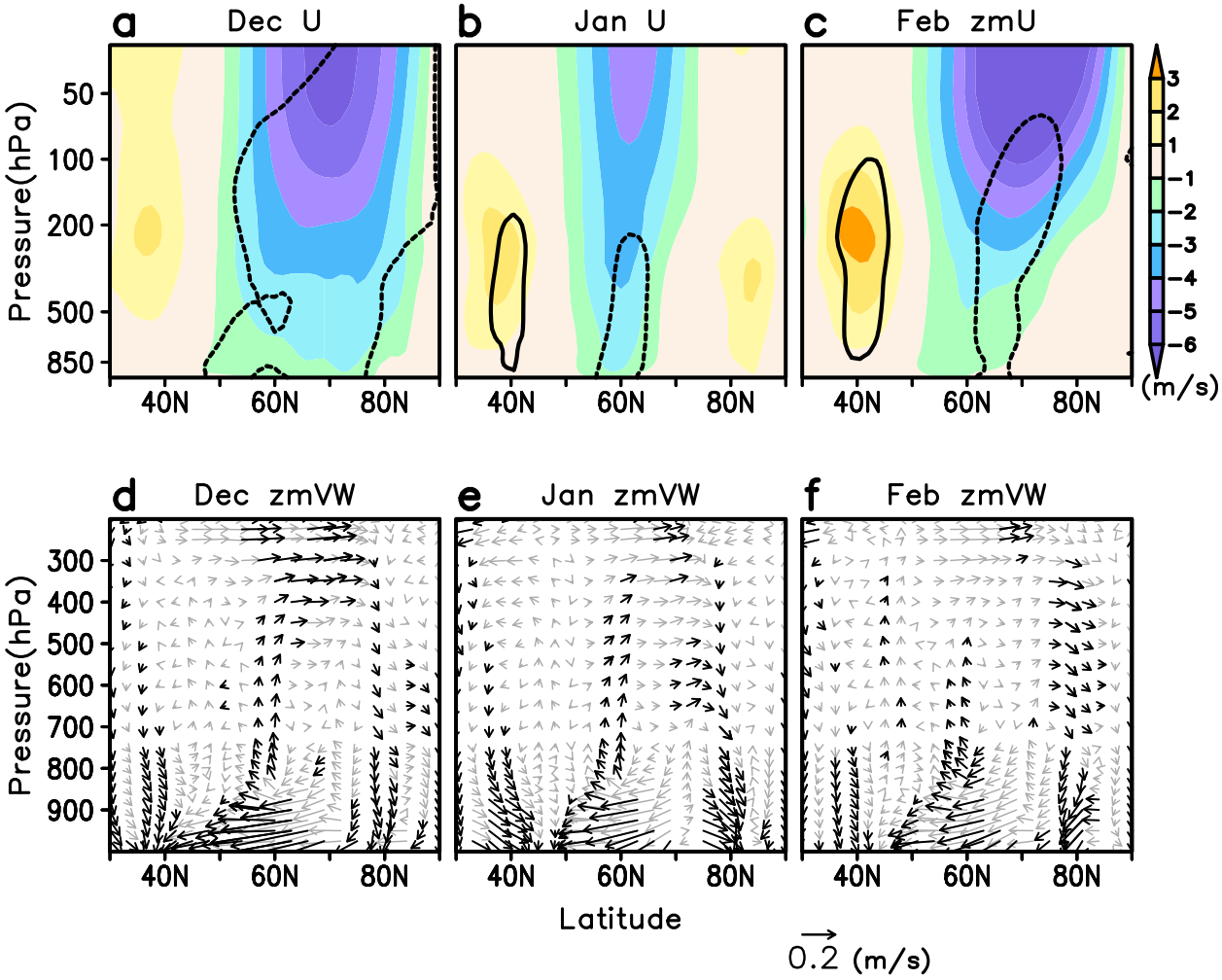

FIG. 7. Composites of zonal-mean zonal wind anomalies in (a) December, (b) January, and (c) February based on the low-minus-high years of hi-NovBASI. Solid (dashed) lines enclose the positive (negative) values that are significant at the 95% confidence level. (d)–(f) As in (a)–(c), but for composites of the mean meridional circulation. The vertical velocity anomalies are amplified by 10-fold. Black vectors denote either the meridional or the vertical velocity anomalies exceeding the 95% confidence level.

followed by a significant relaxation of the stratospheric polar nighttime jet (Fig. 6c) and the reestablishment of the tropospheric dipole pattern in February (Fig. 9a). The mechanism for the establishment of the dipole zonal wind pattern and stratosphere–troposphere coupling can be interpreted in the framework of wave–mean flow interaction, as discussed below.

5. Wave–mean flow interaction

The mean zonal circulation climatology in January is characterized by the coexistence of the tropospheric jet stream (at ~30°N and 200 hPa) and the stratospheric polar nighttime jet (at ~65°N and 10 hPa), as shown in Fig. 9d (thin contours). Because of persistent deceleration of the tropospheric westerly at 60°N latitude (Fig. 7b), the meridional gradient of zonal winds intensifies at the poleward flank of the tropospheric jet stream (Fig. 9d, color shading). The intensified gradient of zonal wind represents the increase of horizontal wind shear, by virtue of which the zonal mean flow becomes barotropic instability. The barotropic instability favors the energy cascading from the mean flow to smaller-scale waves or eddies, providing a source of energy for the waves and eddies (Vallis 2006).

Previous studies have shown the impact of Arctic sea ice on the cold Eurasian winter weather extremes, polar vortex weakening, and negative AO, all of which are partially related to the change in planetary wave propagation (Dethloff et al. 2006; Honda et al. 2009; Francis and Vavrus 2012; Screen and Simmonds 2014; Kim et al. 2014; Peings and Magnusdottir 2014). There are also

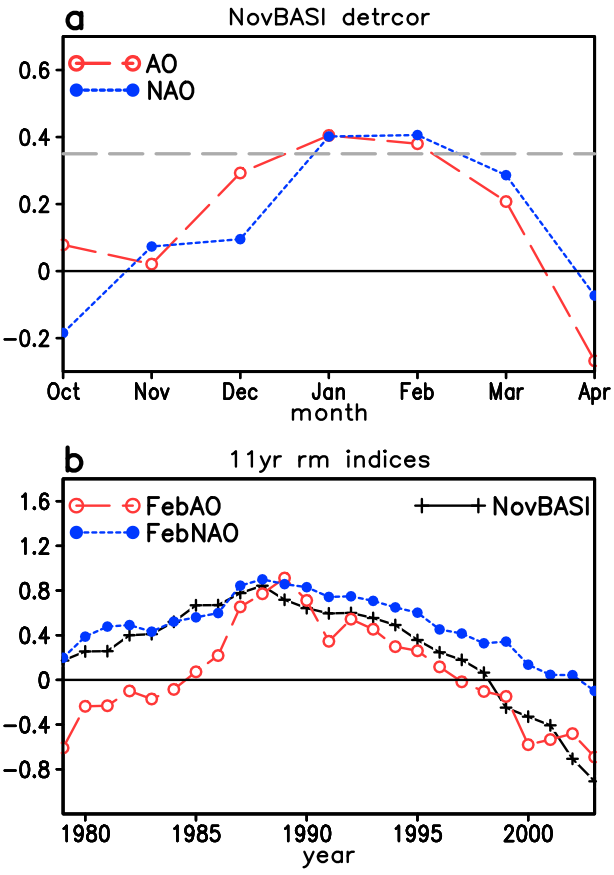

FIG. 8. (a) Correlation coefficients between detrended NovBASI and AO (red) and NAO (blue) indices. The dashed gray line denotes the 95% significance level. (b) The 11-yr running mean time series of the NovBASI and February AO and NAO indices. The horizontal axis represents the starting year of the 11-yr mean.

indications that the sea ice anomalies can influence synoptic-scale eddy activity through changes in the storm track (Singarayer et al. 2006; Inoue et al. 2012; Orsolini et al. 2012). Jaiser et al. (2012) suggested that Arctic sea ice change impacts differently the development of synoptic and planetary waves. Those studies, though implicating the significance of eddies in the remote impact of sea ice, did not articulate the processes involving the two-way interaction between the mean flows and waves. Given their possible roles in the teleconnection of the sea ice anomalies and remote atmospheric responses, the stationary and transient EP fluxes and their divergence on the pressure–latitude sections are composited based on the hi-NovBASI. The November anomalous upward stationary wave EP flux (representing poleward heat flux) associated with the November low-minus-high BK sea ice is located at approximately 70°N, which corresponds to enhanced northward heat flux and thus contributes to the surface Arctic warming (figure not shown). However, the transient EP flux counteracts the effect of stationary waves by reducing the poleward heat flux at the same latitudes (figure not shown). The delayed responses of EP flux and its divergence from December to February are presented in Fig. 10. There are anomalous poleward EP fluxes of both stationary waves and transient eddies in the upper troposphere. The anomalous EP flux convergence (divergence) arises at the poleward of about 60°N (equatorward of about 40°N) flank of the maximal horizontal EP flux anomalies at the upper-tropospheric levels. According to wave–mean flow interaction theory, these EP flux convergence (divergence) anomalies tend to decelerate (accelerate) the mean flow (Vallis 2006). Therefore, the westerlies increase equatorward of 50°N and decrease poleward of 50°N, creating a dipole pattern in the troposphere. In addition, the negative anomaly of hi-NovBASI is followed by the strong prevailing upward propagation of stationary wave energy from the upper troposphere to the lower stratosphere in January (Fig. 10b), which may, to some extent, disturb the stratospheric circulation.

Further examination of the detailed processes of AO mode development was rendered by dissecting the zonal wind dipole pattern into the time–pressure sections of 50°–70°N mean composites (Fig. 11a) and 30°–45°N mean composites (Fig. 11c), respectively. A number of factors (e.g., the upper-tropospheric EP flux divergence, the lower-tropospheric meridional wind, and the vertical component of EP flux at the tropopause level) contribute to the zonal wind anomalies (Figs. 11b,d). Corresponding to the BK sea ice retreat, the lower-stratospheric polar nighttime jet decelerate remarkably in late November. The stratospheric zonal wind anomalies propagate downward to the troposphere in late December and early January. The largest zonal wind deceleration coincides sequentially with first the significant EP flux convergence anomalies at the upper troposphere (black line in Fig. 11b) and then the anomalous northerly wind at the lower troposphere (green line in Fig. 11b), which are associated with the speedup of the polar cell (Fig. 7d–f). As mentioned above, EP flux convergence acts to decelerate the zonal-mean zonal flow, and the northerly anomalies tend to produce the easterly anomalies in the NH under the Coriolis effect. These two factors collaborate to drive the subpolar deceleration of zonal wind from the surface to tropopause. Such westerly deceleration brings about an increase of midlatitude (40°–60°N) horizontal wind shear (Fig. 9d). The subsequently intensified mean flow barotropic instability may account for the intensified planetary wave activity and hence the significant upward stationary EP flux anomalies at the tropopause level in January (red line in Fig. 11b). The enhanced wave disturbances from the troposphere to stratosphere are the harbingers of the

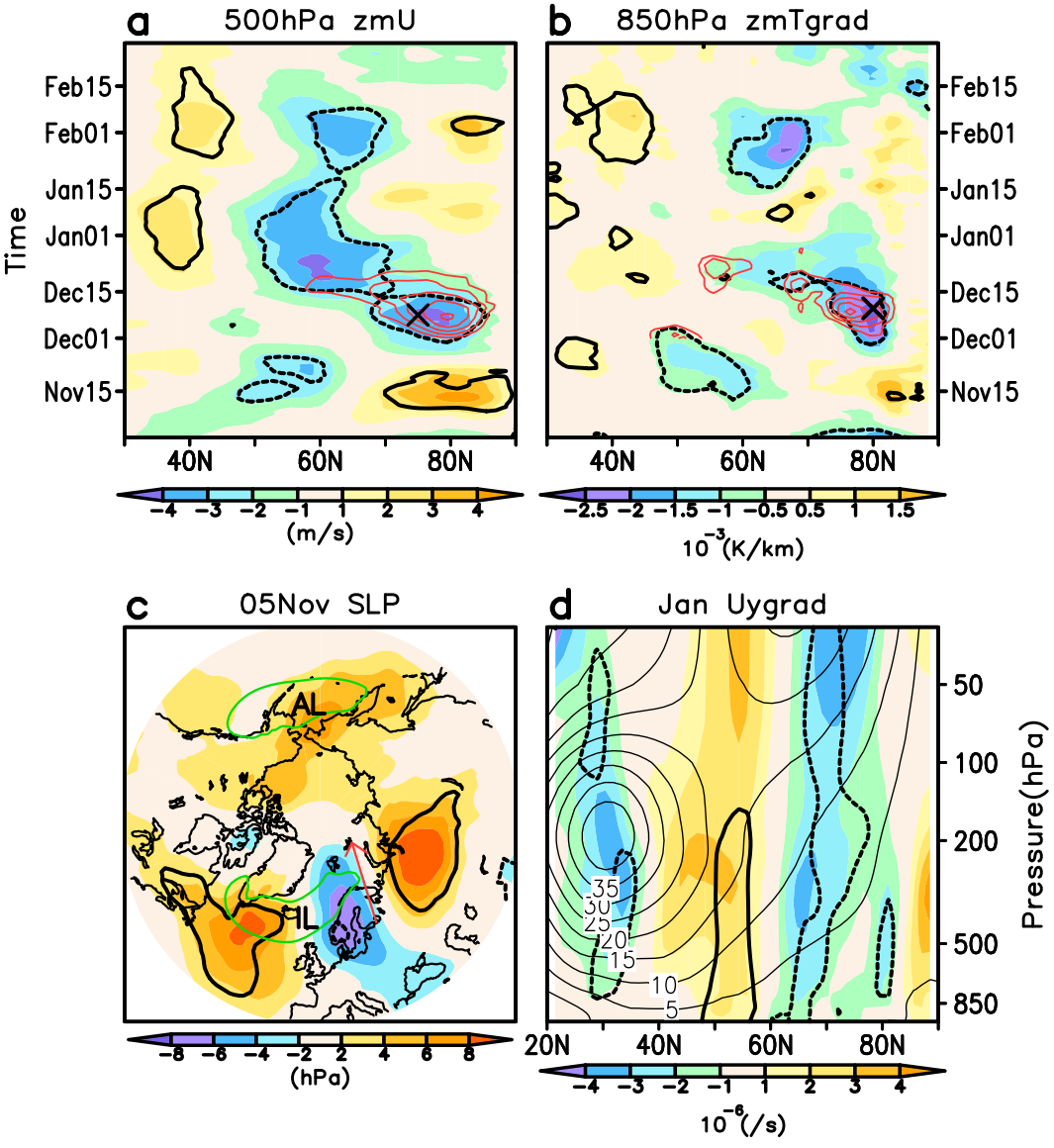

FIG. 9. (a) Composites of the 15-day low-pass filtered zonal-mean zonal wind at the 500-hPa level based on the hi-NovBASI (low-minus-high years). The red contours denote the lead–lag correlations between the 500-hPa zonal-mean zonal wind and the 850-hPa meridional temperature gradient on 10 December at 80°N, as marked by the cross in (b). Contour intervals are 0.3, 0.4, 0.5, 0.6, and 0.7. (b) As in (a), but for the 850-hPa meridional temperature gradient. The red contours denote the lead–lag correlations between the 850-hPa meridional temperature gradient and the 500-hPa zonal-mean zonal wind 8 December at 75°N, as marked by the cross in (a). Contour intervals are 0.3, 0.4, 0.5, 0.6, and 0.7. (c) Composites of 5 November sea level pressure anomalies based on the hi-NovBASI (low-minus-high years). The green contours mark the climatological location of Icelandic low and Aleutian low. The red arrow indicates the northward warm advection over the BK Seas. (d) Composites of January meridional gradient of the zonal wind anomalies based on the hi-NovBASI (color shading). Positive (negative) values indicate the enhanced (reduced) south–north wind shear. Thick solid (dashed) lines enclose the positive (negative) values that are significant at the 95% confidence level. The January zonal-mean zonal wind climatology is also shown as the thin black contours ($m\,s^{-1}$), with the maximum in the upper-tropospheric (lower stratospheric) level signifying the location of the subtropical jet stream (polar nighttime jet).

stratospheric polar vortex weakening and sudden stratospheric warming (Polvani and Waugh 2004), which are closely connected to the relaxation of the stratospheric polar nighttime jet in late January (Fig. 11a). The zonal wind anomalous signals again propagate downward from the stratosphere to troposphere on a time scale of about 20 days. In the meanwhile, the upper-tropospheric EP flux convergence and the lower-tropospheric northerly wind anomalies reemerge in February. The tropospheric zonal wind deceleration acts in concert with the downward

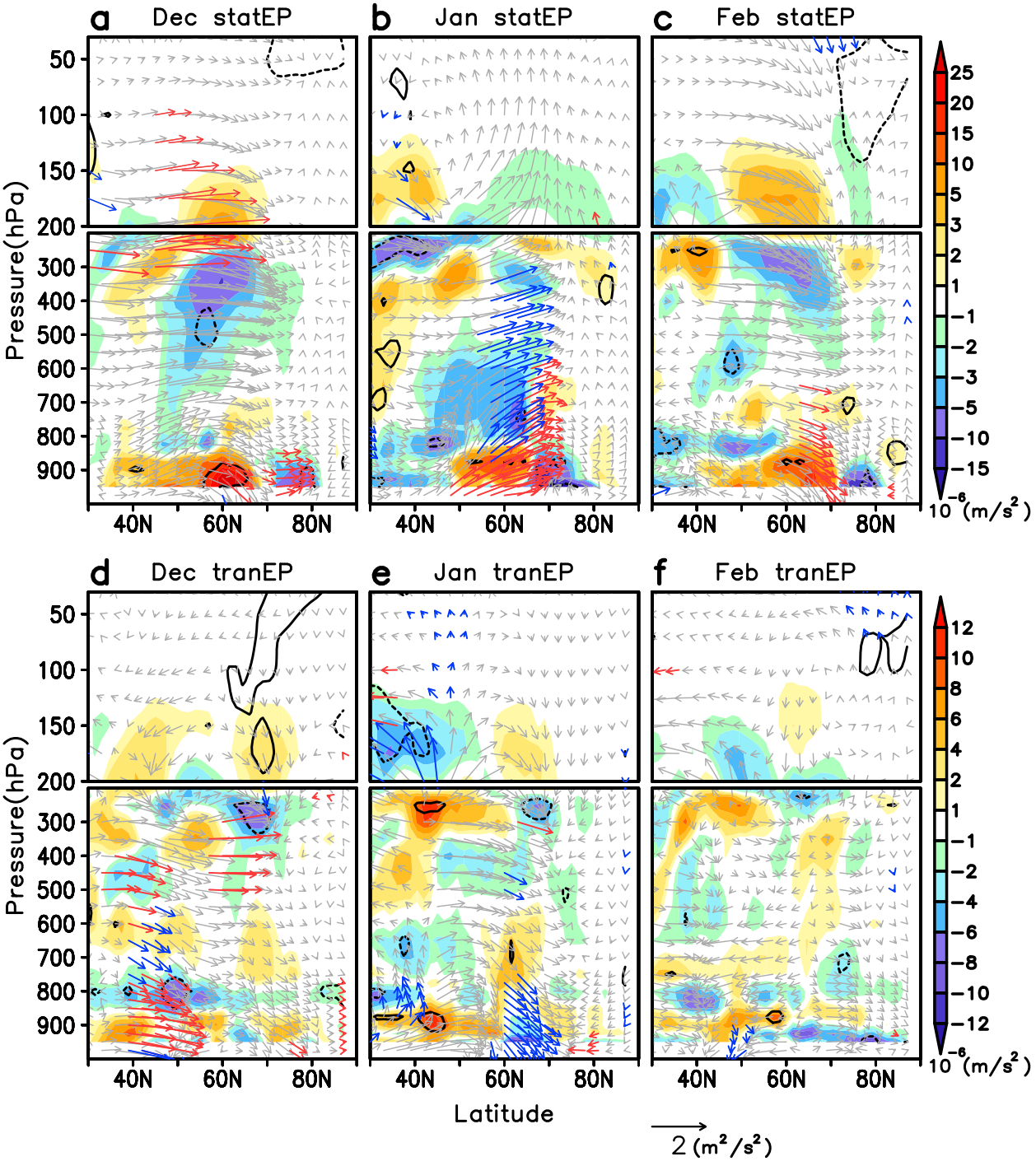

FIG. 10. Composites of the stationary wave EP flux (vector) and EP flux divergence (color shading) anomalies in (a) December, (b) January, and (c) February based on the hi-NovBASI low-minus-high years. The positive (negative) values in color shading denote the EP flux divergence (convergence) anomalies. (d)–(f) As in (a)–(c), but for composites of the transient eddy EP flux and its divergence. EP flux divergence (convergence) values significant at the 95% confidence level are enclosed by the solid (dashed) lines. Blue (red) vectors are the vertical (meridional) EP flux anomalies that exceed the 95% significance level.

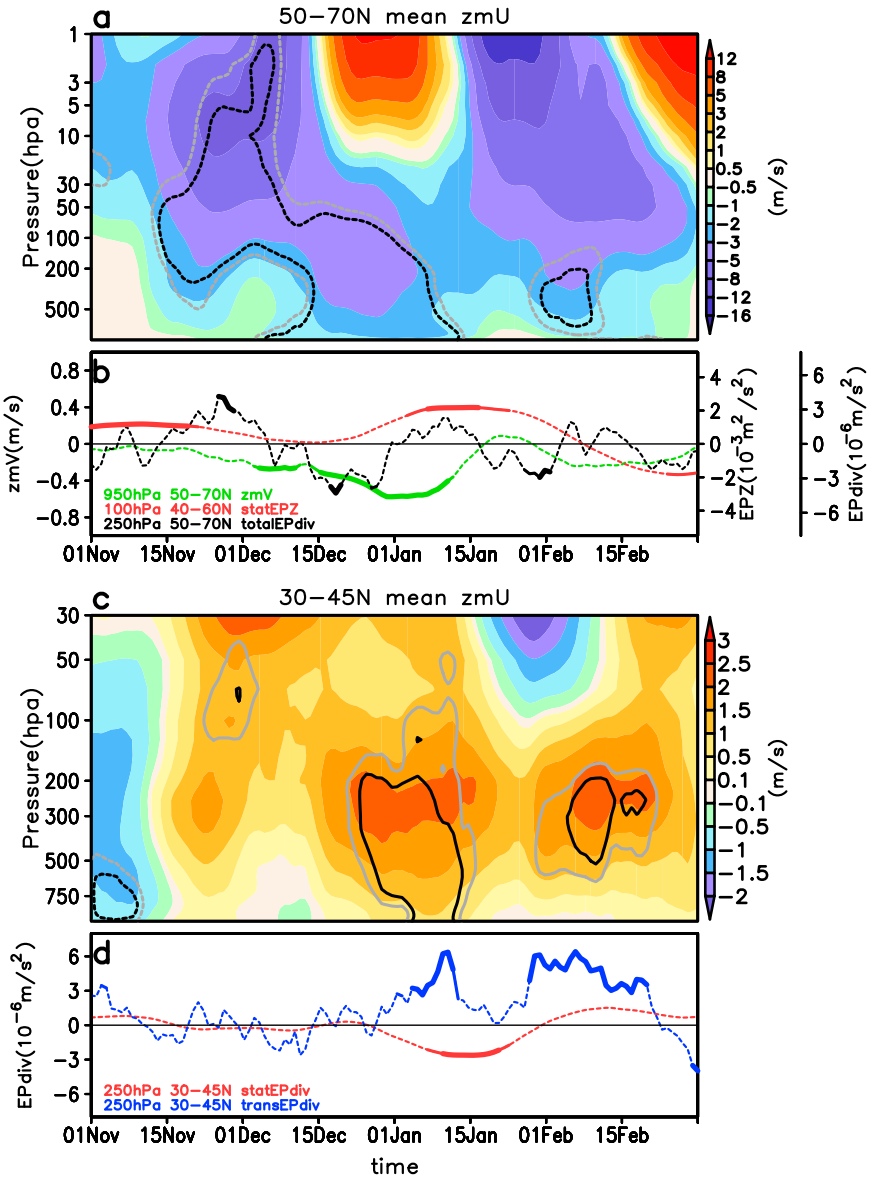

FIG. 11. (a) Composites of the 15-day low-pass 50°–70°N mean zonal-mean zonal wind based on hi-NovBASI low-minus-high years. Black (gray) contours enclose the values that are significant at the 95% (90%) confidence level. (b) Composites of the 100-hPa stationary vertical EP flux (red, right axis), the 950-hPa zonal-mean meridional wind (green, left axis), and the 250-hPa total EP flux divergence (black, far right axis). The positive (negative) values of black line denote the EP flux divergence (convergence) anomalies. (c) As in (a), but for the 30°–45°N mean zonal-mean zonal wind. (d) Composites of the 250-hPa stationary (red) and transient (blue) EP flux divergence. Thick solid lines in (b) and (d) mark the values exceeding the 95% level.

propagation of zonal wind signals from the lower stratosphere, achieving the coupling between the stratosphere and troposphere in February. It is noteworthy that the stratosphere–troposphere coupling appears not only in February but also in late November–early December (Fig. 11a), following the anomalous upward wave energy propagation in early November (Fig. 11b). The concurrence of this coupling process at the upper troposphere–lower stratosphere and the BK sea ice decline at the air–sea interface eliminates the possible causal link between them. The apparent correlation may be attributed to other factors currently unknown to us.

Aside from contributing to the zonal wind deceleration, the near-surface northerly wind anomalies

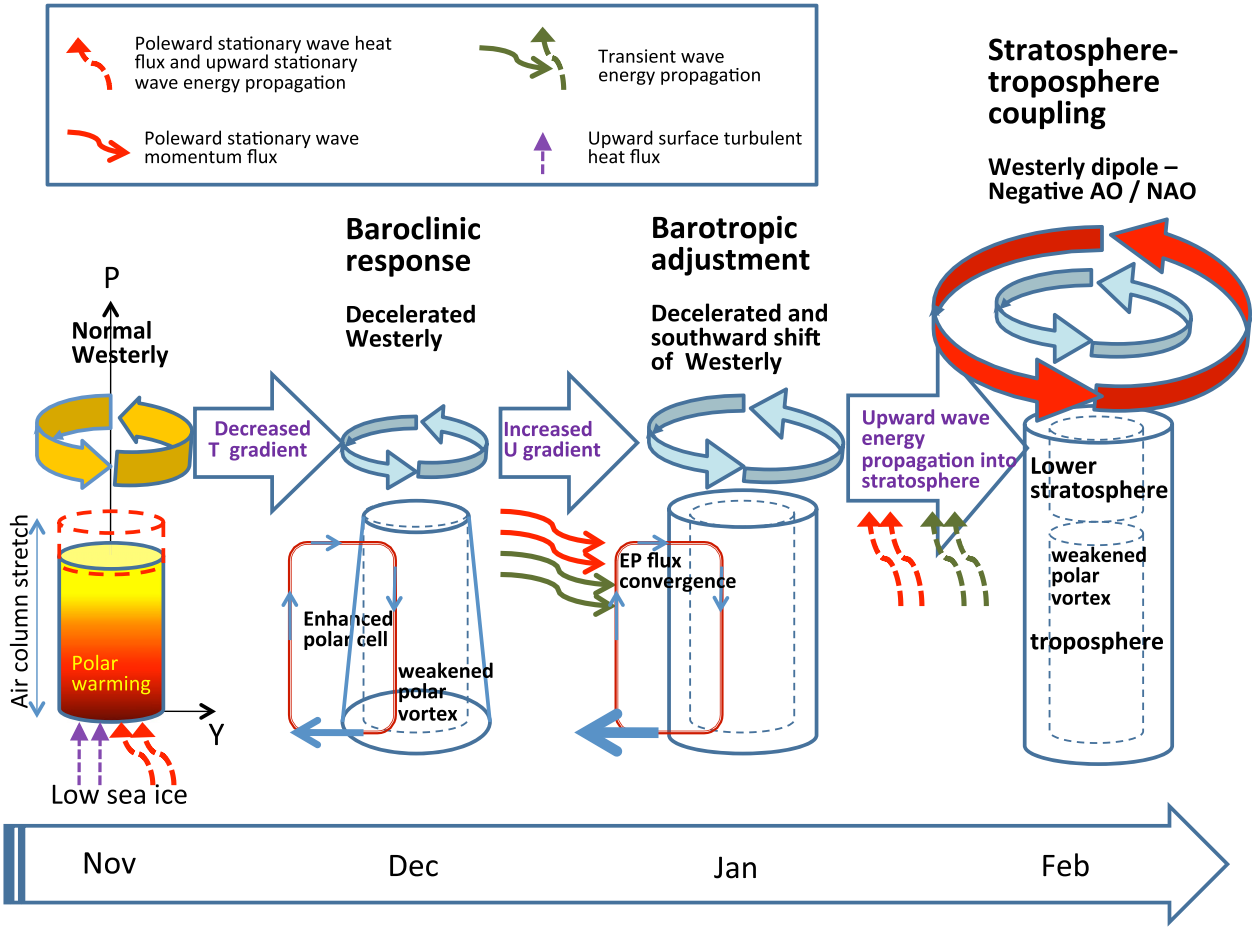

FIG. 12. Schematic diagram depicting the winter atmospheric circulation response to the November BK sea ice retreat. The seasonal evolution from November to February is marked across the bottom, with by the corresponding atmospheric circulation responses above, and the cylinders denoting the polar air columns. The key processes responsible for transmitting the atmospheric anomalous signals through time are labeled within the big blue arrows. Normal, decelerated, and accelerated westerlies are shown as yellow, blue, and red circular arrows, respectively.

themselves may, to some extent, be attributed to the wave activity, as evidenced by the fact that significant northerly wind anomalies closely follow the negative anomalies of total EP flux divergence (Fig. 11b). To offset the eddy effect on the deceleration of zonal wind at the subpolar upper troposphere, the large-scale atmospheric circulation tends to adjust itself and induce a local counterclockwise meridional circulation (Holton and Hakim 2013), hence fueling the speedup of the meridional polar cell and the corresponding lower-tropospheric northerly wind anomalies.

Compared with the subpolar region, the subtropical positive zonal wind anomalies are located primarily at the middle-to-upper-tropospheric levels (Fig. 11c). The transient EP flux divergence is the major factor contributing to the zonal wind acceleration, while stationary EP flux acts to cancel out the transient eddy effect in January and reinforce the transient eddy effect in February (Fig. 11d). The stratosphere–troposphere coupling process and the establishment of the tropospheric zonal wind dipole pattern both demonstrate the robust dynamic linkage between November BK sea ice and the AO mode.

6. Conclusions and discussion

In this study, the critical timing and location of Arctic sea ice forcing on the winter atmospheric circulation are determined in terms of consistency among sea ice loss, surface turbulent heat flux, and Arctic warming, both in the interannual variances and long-term trends. The November BK sea ice retreat not only plays a significant role in the recent Arctic warming, but it also leads to changes in the large-scale atmospheric circulation. The sequential dynamical processes linking the November BK sea ice retreat to the negative AO phase in February were conceptually illustrated in Fig. 12. The immediate

reaction of the atmosphere to sea ice loss is the thermodynamic polar air column stretching and lower-level warming. The subsequent decrease of the meridional temperature gradient induces the deceleration and southward shift of the circumpolar westerly in the troposphere and the intensification of the meridional polar cell in December. The large-scale atmospheric response in December stimulates the wave–mean flow interaction in the following months: the enhanced midlatitude barotropic instability due to increasing horizontal wind shear facilitates the EP flux convergence of both stationary wave and transient eddies at the subpolar latitudes, which induce the deceleration of zonal wind in the upper troposphere. The persistent northerly wind anomalies continuously feed back to the deceleration of zonal winds in the lower troposphere. Synchronous deceleration of zonal wind throughout the troposphere represents the barotropic adjustment processes of the atmospheric circulation in January. The enhanced upward stationary wave energy propagation contributes to the lower-stratospheric warming and polar vortex weakening in late January and February. Through the stratosphere–troposphere coupling and downward propagation of zonal wind anomalies, the negative AO pattern reaches its peak amplitude in February.

Our study, consistent with Jaiser et al. (2012), proposed that the sea ice anomalies can exert a remote impact on the winter atmospheric circulation through the atmospheric dynamical adjustment processes. However, Jaiser et al. (2012) focused on the late summer season (August–September) and the Siberian domain, when and where the sea ice exhibits both strong standard deviation and linear decreasing trends [see Fig. 1 from Jaiser et al. (2012)]. However, melting in the late summer cannot directly force the atmosphere, because heat fluxes are going into the ocean from the atmosphere in this season. When heat transfers from the ocean to the atmosphere in fall (and is particularly strong in winter) sea ice anomalies provide a forcing to the atmosphere. Only the Barents–Kara Seas sustain the sea ice variation and significant declining trends in the cold season (Fig. 1b), which highlights the importance of the sea ice anomalies in the Barents–Kara Seas to the winter atmospheric circulation. In summary, this study makes new contributions in two areas: First, we explained why the Barents and Kara Seas are the key area and why November is the critical month for sea ice influencing the winter atmosphere. The BK seas are the only area within the Arctic Circle where sea ice exhibits large variability and long-term trends throughout winter (Fig. 1b), which allows sea ice to exert tremendous influences on the overlying atmosphere through surface fluxes. The net turbulent flux in the BK Seas shows the largest variability and long-term trend in November (Fig. 1c), which makes this month a likely window to initialize surface disturbance to the atmosphere. Considering the persistence of the sea ice anomaly, such a surface forcing could last through winter. Second, we examined possible physical processes that link sea ice–associated surface fluxes to the responding atmosphere circulation from the troposphere to stratosphere and from the Arctic to midlatitudes. As mentioned above, the deceleration of the subpolar westerly can be attributed by the Arctic warming and intensification of the polar cell, which are both induced by low Arctic sea ice. These thermodynamic and dynamic processes work to reenforce each other. The subsequent wind shear changes lead to the enhanced midlatitude barotropic instability that provides energy for stationary waves and transient eddies. The convergence/divergence of wave flux further impacts the zonal wind distribution. This study proposes a more complete dynamic pathway leading from November sea ice anomalies in the BK Seas to February AO variability than that presented in Cohen et al. (2014a).

It is well known that the winter AO index has exhibited a significant downward trend since the 1990s (Overland and Wang 2005), and its spatial pattern shifted from the traditional tripolar pattern to a dipole pattern (Zhang et al. 2008). Our study is consistent with previous studies by acknowledging the role of early winter sea ice variability in the Barents and Kara Seas in leading the recent weakening of the winter AO/NAO mode (Kim et al. 2014; Inoue et al. 2012). In addition, we demonstrate how this connection happens and identify the possible dynamic responses in each month from November to February.

In addition to the changing greenhouse gas forcing, BK sea ice is another important factor in influencing the northern middle-to-high-latitude climate change but is not the only factor. The Eurasian snow cover (Cohen et al. 2014b) and tropical Pacific SST anomalies (Ding et al. 2014) have also contributed to the recent NH climate change. On the other hand, Cattiaux and Cassou (2013) compared the winter AO changes estimated from previous (CMIP3) versus ongoing (CMIP5) generations of multimodel projections under similar emission scenarios. They found a large discrepancy between the two model groups in predicting the AO trends, with positive AO trends in CMIP3 but negative AO trends in CMIP5. The probable causes may include whether the models correctly simulate the localized faster sea ice loss in the Barents and Kara Seas in early winter and whether the models are effective in simulating the dynamic responses in the atmosphere, as we suggested here. It could also depend on whether the models correctly capture the remote influence of the western tropical Pacific warming in late winter. Therefore, the improvement of modeling performance in terms of future northern extratropical climate prediction may depend on gaining a better

understanding of atmospheric responses to various external forcing and on improving simulations of the November BK sea ice trend and variability as well as of the related atmospheric dynamic processes.

Acknowledgments. X.-Y. Yang is supported by the Natural Science Foundation of China (Grant 41576178), the National Basic Research Program of China (2012CB417402), and the Fundamental Research Funds for the Central Universities. Yuan and Ting are supported by the Office of Naval Research (Grant N00014-12-1-0911).

REFERENCES

Alexander, M. A., U. S. Bhatt, J. E. Walsh, M. S. Timlin, J. S. Miller, and J. D. Scott, 2004: The atmospheric response to realistic Arctic sea ice anomalies in an AGCM during winter. *J. Climate*, **17**, 890–905, doi:10.1175/1520-0442(2004)017<0890:TARTRA>2.0.CO;2.

Ambaum, M. H. P., B. J. Hoskins, and D. B. Sephenson, 2001: Arctic Oscillation or North Atlantic Oscillation? *J. Climate*, **14**, 3495–3507, doi:10.1175/1520-0442(2001)014<3495:AOONAO>2.0.CO;2.

Andreas, E. L, 1980: Estimation of heat and mass fluxes over Arctic leads. *Mon. Wea. Rev.*, **108**, 2057–2063, doi:10.1175/1520-0493(1980)108<2057:EOHAMF>2.0.CO;2.

Årthun, M., R. B. Ingvaldsen, L. H. Smedsrud, and C. Schrum, 2011: Dense water formation and circulation in the Barents Sea. *Deep-Sea Res. I*, **58**, 801–817, doi:10.1016/j.dsr.2011.06.001.

——, T. Eldevik, L. H. Smedsrud, Ø. Skagseth, and R. B. Ingvaldsen, 2012: Quantifying the influence of Atlantic heat on Barents Sea ice variability and retreat. *J. Climate*, **25**, 4736–4743, doi:10.1175/JCLI-D-11-00466.1.

Bader, J., M. D. S. Mesquita, K. I. Hodges, N. Keenlyside, S. Østerhus, and M. Miles, 2011: A review on Northern Hemisphere sea-ice, storminess and the North Atlantic Oscillation: Observations and projected changes. *Atmos. Res.*, **101**, 809–834, doi:10.1016/j.atmosres.2011.04.007.

Baldwin, M. P., and T. J. Dunkerton, 2001: Stratospheric harbingers of anomalous weather regimes. *Science*, **294**, 581–584, doi:10.1126/science.1063315.

Barnes, E. A., 2013: Revisiting the evidence linking Arctic amplification to extreme weather in midlatitudes. *Geophys. Res. Lett.*, **40**, 4728–4733, doi:10.1002/grl.50880.

Bretherton, C. S., M. Widmann, V. P. Dynmikov, J. M. Wallace, and I. Bladé, 1999: The effective number of spatial degrees of freedom of a time-varying field. *J. Climate*, **12**, 1990–2009, doi:10.1175/1520-0442(1999)012<1990:TENOSD>2.0.CO;2.

Budikova, D., 2009: Role of Arctic sea ice in global atmospheric circulation: A review. *Global Planet. Change*, **68**, 149–163, doi:10.1016/j.gloplacha.2009.04.001.

Cattiaux, J., and C. Cassou, 2013: Opposite CMIP3/CMIP5 trends in the wintertime Northern Annular Mode explained by combined local sea ice and remote tropical influences. *Geophys. Res. Lett.*, **40**, 3682–3687, doi:10.1002/grl.50643.

Cavalieri, D. J., C. L. Parkinson, P. Gloersen, and H. J. Zwally, 2013: Sea ice concentrations from *Nimbus-7* SMMR and DMSP SSM/I-SSMIS passive microwave data, version 1. National Snow and Ice Data Center, accessed March 2014. [Available online at http://nsidc.org/data/nsidc-0051.html.]

Cohen, J., M. Barlow, P. J. Kushner, and K. Saito, 2007: Stratosphere–troposphere coupling and links with Eurasian land surface variability. *J. Climate*, **20**, 5335–5343, doi:10.1175/2007JCLI1725.1.

——, and Coauthors, 2014a: Recent Arctic amplification and extreme mid-latitude weather. *Nat. Geosci.*, **7**, 627–637, doi:10.1038/ngeo2234.

——, J. C. Furtado, J. Jones, M. Barlow, D. Whittleston, and D. Entekhabi, 2014b: Linking Siberian snow cover to precursors of stratospheric variability. *J. Climate*, **27**, 5422–5432, doi:10.1175/JCLI-D-13-00779.1.

Comiso, J. C., C. L. Parkinson, R. Gersten, and L. Stock, 2008: Accelerated decline in the Arctic sea ice cover. *Geophys. Res. Lett.*, **35**, L01703, doi:10.1029/2007GL031972.

Dee, D. P., and Coauthors, 2011: The ERA-Interim reanalysis: Configuration and performance of the data assimilation system. *Quart. J. Roy. Meteor. Soc.*, **137**, 553–597, doi:10.1002/qj.828.

Deser, C., G. Magnusdottir, R. Saravanan, and A. Phillps, 2004: The effects of North Atlantic SST and sea ice anomalies on the winter circulation in CCM3. Part II: Direct and indirect components of the response. *J. Climate*, **17**, 877–889, doi:10.1175/1520-0442(2004)017<0877:TEONAS>2.0.CO;2.

——, R. Tomas, and S. Peng, 2007: The transient atmospheric circulation response to North Atlantic SST and sea ice anomalies. *J. Climate*, **20**, 4751–4767, doi:10.1175/JCLI4278.1.

——, ——, M. Alexander, and D. Lawrence, 2010: The seasonal atmospheric response to projected Arctic sea ice loss in the late twenty-first century. *J. Climate*, **23**, 333–351, doi:10.1175/2009JCLI3053.1.

Dethloff, K., and Coauthors, 2006: A dynamical link between the Arctic and the global climate system. *Geophys. Res. Lett.*, **33**, L03703, doi:10.1029/2005GL025245.

Ding, Q., J. M. Wallace, D. S. Battisti, E. J. Steig, A. J. E. Gallant, H.-J. Kim, and L. Geng, 2014: Tropical forcing of the recent rapid Arctic warming in northeastern Canada and Greenland. *Nature*, **509**, 209–212, doi:10.1038/nature13260.

Francis, J. A., and E. Hunter, 2007: Drivers of declining sea ice in the Arctic winter: A tale of two seas. *Geophys. Res. Lett.*, **34**, L17503, doi:10.1029/2007GL030995.

——, and S. J. Vavrus, 2012: Evidence linking Arctic amplification to extreme weather in mid-latitudes. *Geophys. Res. Lett.*, **39**, L06801, doi:10.1029/2012GL051000.

——, W. Chan, D. J. Leathers, J. R. Miller, and D. E. Veron, 2009: Winter Northern Hemisphere weather patterns remember summer Arctic sea-ice extent. *Geophys. Res. Lett.*, **36**, L07503, doi:10.1029/2009GL037274.

Holton, J. R., and G. J. Hakim, 2013: Middle atmosphere dynamics. *An Introduction to Dynamic Meteorology*, 5th ed. International Geophysics Series, Vol. 88, Academic Press, 407–447.

Honda, M., J. Inoue, and S. Yamane, 2009: Influence of low Arctic sea-ice minima on anomalously cold Eurasian winters. *Geophys. Res. Lett.*, **36**, L08707, doi:10.1029/2008GL037079.

Inoue, J., M. E. Hori, and K. Takaya, 2012: The role of Barents Sea ice in the wintertime cyclone track and emergence of a warm-Arctic cold-Siberian anomaly. *J. Climate*, **25**, 2561–2568, doi:10.1175/JCLI-D-11-00449.1.

Jaiser, R., K. Dethloff, D. Handorf, A. Rinke, and J. Cohen, 2012: Impact of sea ice cover changes on the Northern Hemisphere atmospheric winter circulation. *Tellus*, **64A**, 11 595, doi:10.3402/tellusa.v64i0.11595.

Kim, B.-M., S.-W. Son, S.-K. Min, J.-H. Jeong, S.-J. Kim, X. Zhang, T. Shim, and J.-H. Yoon, 2014: Weakening of the stratospheric

polar vortex by Arctic sea-ice loss. *Nature*, **5**, 4646, doi:10.1038/ncomms5646.

Koenigk, T., and L. Brodeau, 2014: Ocean heat transport into the Arctic in the twentieth and twenty-first century in EC-Earth. *Climate Dyn.*, **42**, 3101–3120, doi:10.1007/s00382-013-1821-x.

——, U. Mikolajewicz, J. H. Jungclaus, and A. Kroll, 2009: Sea ice in the Barents Sea: Seasonal to interannual variability and climate feedbacks in a global coupled model. *Climate Dyn.*, **32**, 1119–1138, doi:10.1007/s00382-008-0450-2.

——, M. Caian, G. Nikulin, and S. Schimanke, 2015: Regional Arctic sea ice variations as predictor for winter climate conditions. *Climate Dyn.*, **46**, 317–337, doi:10.1007/s00382-015-2586-1.

Liptak, J., and C. Strong, 2014: The winter atmospheric response to sea ice anomalies in the Barents Sea. *J. Climate*, **27**, 914–924, doi:10.1175/JCLI-D-13-00186.1.

Magnusdottir, G., C. Deser, and R. Saravanan, 2004: The effect of North Atlantic SST and sea ice anomalies on the winter circulation in CCM3. Part I: Main features and storm track characteristics of the response. *J. Climate*, **17**, 857–876, doi:10.1175/1520-0442(2004)017<0857:TEONAS>2.0.CO;2.

Massonnet, F., T. Fichefet, H. Goosse, C. M. Bitz, G. Philippon-Berthier, M. M. Holland, and P.-Y. Barriat, 2012: Constraining projections of summer Arctic sea ice. *Cryosphere*, **6**, 1383–1394, doi:10.5194/tc-6-1383-2012.

Mori, M., M. Watanabe, H. Shiogama, J. Inoue, and M. Kimoto, 2014: Robust Arctic sea-ice influence on the frequent Eurasian cold winters in past decades. *Nat. Geosci.*, **7**, 869–873, doi:10.1038/ngeo2277.

Murray, R. J., and I. Simmonds, 1995: Response of climate and cyclones to reductions in Arctic winter sea ice. *J. Geophys. Res.*, **100**, 4791–4806, doi:10.1029/94JC02206.

Orsolini, Y. J., R. Senan, R. E. Benestad, and A. Melsom, 2012: Autumn atmospheric response to the 2007 low Arctic sea ice extent in coupled ocean–atmosphere hindcasts. *Climate Dyn.*, **38**, 2437–2448, doi:10.1007/s00382-011-1169-z.

Overland, J. E., and M. Wang, 2005: The Arctic climate paradox: The recent decrease of the Arctic Oscillation. *Geophys. Res. Lett.*, **32**, L06701, doi:10.1029/2004GL021752.

——, and ——, 2010: Large-scale atmospheric circulation changes are associated with the recent loss of Arctic sea ice. *Tellus*, **62A**, 1–9, doi:10.1111/j.1600-0870.2009.00421.x.

——, K. R. Wood, and M. Wang, 2011: Warm Arctic–cold continents: Climate impacts of the newly open Arctic Sea. *Polar Res.*, **30**, 15 787, doi:10.3402/polar.v30i0.15787.

Peings, Y., and G. Magnusdottir, 2014: Response of the wintertime Northern Hemisphere atmosphere circulation to current and projected Arctic sea ice decline: A numerical study with CAM5. *J. Climate*, **27**, 244–264, doi:10.1175/JCLI-D-13-00272.1.

Petoukhov, V., and V. A. Semenov, 2010: A link between reduced Barents–Kara Sea ice and cold winter extremes over northern continents. *J. Geophys. Res.*, **115**, D21111, doi:10.1029/2009JD013568.

Polvani, L. M., and D. W. Waugh, 2004: Upward wave activity flux as a precursor to extreme stratospheric events and subsequent anomalous surface weather regimes. *J. Climate*, **17**, 3548–3554, doi:10.1175/1520-0442(2004)017<3548:UWAFAA>2.0.CO;2.

Polyakov, I. V., and Coauthors, 2003: Long-term ice variability in Arctic marginal seas. *J. Climate*, **16**, 2078–2085, doi:10.1175/1520-0442(2003)016<2078:LIVIAM>2.0.CO;2.

——, and Coauthors, 2004: Variability of the intermediate Atlantic water of the Arctic Ocean over the last 100 years. *J. Climate*, **17**, 4485–4497, doi:10.1175/JCLI-3224.1.

Rigor, I. G., J. M. Wallace, and R. L. Colony, 2002: Response of sea ice to the Arctic Oscillation. *J. Climate*, **15**, 2648–2663, doi:10.1175/1520-0442(2002)015<2648:ROSITT>2.0.CO;2.

Santer, B. D., T. M. L. Wigley, J. S. Boyle, D. J. Gaffen, J. Hnilo, D. Nychka, D. E. Parker, and K. E. Taylor, 2000: Statistical significance of trends and trend differences in layer-average atmospheric temperature time series. *J. Geophys. Res.*, **105**, 7337–7356, doi:10.1029/1999JD901105.

Sato, K., J. Inoue, and M. Watanabe, 2014: Influence of the Gulf Stream on the Barents Sea ice retreat and Eurasian coldness during early winter. *Environ. Res. Lett.*, **9**, 084009, doi:10.1088/1748-9326/9/8/084009.

Schauer, U., H. Loeng, B. Rudels, V. K. Ozhigin, and W. Dieck, 2002: Atlantic water flow through the Barents and Kara Seas. *Deep-Sea Res. I*, **49**, 2281–2298, doi:10.1016/S0967-0637(02)00125-5.

Screen, J. A., and I. Simmonds, 2010: The central role of diminishing sea ice in recent Arctic temperature amplification. *Nature*, **464**, 1334–1337, doi:10.1038/nature09051.

——, and ——, 2014: Amplified mid-latitude planetary waves favour particular regional weather extremes. *Nat. Climate Change*, **4**, 704–709, doi:10.1038/nclimate2271.

——, ——, C. Deser, and R. Tomas, 2013: The atmospheric response to three decades of observed Arctic sea ice loss. *J. Climate*, **26**, 1230–1248, doi:10.1175/JCLI-D-12-00063.1.

——, C. Deser, I. Simmonds, and R. Tomas, 2014: Atmospheric impacts of Arctic sea-ice loss, 1979-2009: Separating forced change from atmospheric internal variability. *Climate Dyn.*, **43**, 333–344, doi:10.1007/s00382-013-1830-9.

Seierstad, I. A., and J. Bader, 2009: Impact of a projected future Arctic sea ice reduction on extratropical storminess and the NAO. *Climate Dyn.*, **33**, 937–943, doi:10.1007/s00382-008-0463-x.

Serreze, M. C., M. M. Holland, and J. Stroeve, 2007: Perspectives on the Arctic's shrinking sea ice cover. *Science*, **315**, 1533–1536, doi:10.1126/science.1139426.

Simmonds, I., 2015: Comparing and contrasting the behavior of Arctic and Antarctic sea ice over the 35 year period 1979–2013. *Ann. Glaciol.*, **56**, 18–28, doi:10.3189/2015AoG69A909.

——, and K. Keay, 2009: Extraordinary September Arctic sea ice reductions and their relationships with storm behavior over 1979–2008. *Geophys. Res. Lett.*, **36**, L19715, doi:10.1029/2009GL039810.

Simonsen, K., and P. M. Haugan, 1996: Heat budgets of the Arctic Mediterranean and sea surface heat flux parameterizations for the Nordic Seas. *J. Geophys. Res.*, **101**, 6553–6576, doi:10.1029/95JC03305.

Singarayer, J. S., J. L. Bamber, and P. J. Valdes, 2006: Twenty-first-century climate impacts from a declining Arctic sea ice cover. *J. Climate*, **19**, 1109–1125, doi:10.1175/JCLI3649.1.

Smedsrud, L. H., and Coauthors, 2013: The role of the Barents Sea in the Arctic climate system. *Rev. Geophys.*, **51**, 415–449, doi:10.1002/rog.20017.

Spielhagen, R. F., and Coauthors, 2011: Enhanced modern heat transfer to the Arctic by warm Atlantic water. *Science*, **331**, 450–453, doi:10.1126/science.1197397.

Strey, S. T., W. L. Chapman, and J. E. Walsh, 2010: The 2007 sea ice minimum: Impacts on the Northern Hemisphere atmosphere in late autumn and early winter. *J. Geophys. Res.*, **115**, D23103, doi:10.1029/2009JD013294.

Stroeve, J. C., M. C. Serreze, M. M. Holland, J. E. Kay, J. Malanik, and A. P. Barrett, 2012: The Arctic's rapidly shrinking sea ice cover: A research synthesis. *Climatic Change*, **110**, 1005–1027, doi:10.1007/s10584-011-0101-1.

Strong, C., and G. Magnusdottir, 2011: Dependence of NAO variability on coupling with sea ice. *Climate Dyn.*, **36**, 1681–1689, doi:10.1007/s00382-010-0752-z.

——, ——, and H. Stern, 2009: Observed feedback between winter sea ice and the North Atlantic Oscillation. *J. Climate*, **22**, 6021–6032, doi:10.1175/2009JCLI3100.1.

Thompson, D. W. J., J. M. Wallace, and G. C. Hegerl, 2000: Annular modes in the extratropical circulation. Part II: Trends. *J. Climate*, **13**, 1018–1036, doi:10.1175/1520-0442(2000)013<1018:AMITEC>2.0.CO;2.

Vallis, G. K., 2006: *Atmospheric and Oceanic Fluid Dynamics: Fundamentals and Large-Scale Circulation*. Cambridge University Press, 745 pp.

Vihma, T., 2014: Effects of Arctic sea ice decline on weather and climate: A review. *Surv. Geophys.*, **35**, 1175–1214, doi:10.1007/s10712-014-9284-0.

Wu, Q., and X. Zhang, 2010: Observed forcing-feedback processes between Northern Hemisphere atmospheric circulation and Arctic sea ice coverage. *J. Geophys. Res.*, **115**, D14119, doi:10.1029/2009JD013574.

Yang, X.-Y., and X. Yuan, 2014: The early winter sea ice variability under the recent Arctic climate shift. *J. Climate*, **27**, 5092–5110, doi:10.1175/JCLI-D-13-00536.1.

Zhang, X., M. Ikeda, and J. E. Walsh, 2003: Arctic sea ice and freshwater changes driven by the atmospheric leading mode in a coupled sea ice–ocean model. *J. Climate*, **16**, 2159–2177, doi:10.1175/2758.1.

——, A. Sorteberg, J. Zhang, R. Gerdes, and J. C. Comiso, 2008: Recent radical shifts of atmospheric circulations and rapid changes in Arctic climate system. *Geophys. Res. Lett.*, **35**, L22701, doi:10.1029/2008GL035607.

Zhou, T., and J. Li, 2008: Climate change in China congruent with the linear trends of the Annual Modes. *Atmos. Ocean. Sci. Lett.*, **1**, 1–7.